JES Focus Issue on Progress in Molten Salts and Ionic Liquids

An Electrochemical Quartz Crystal Microbalance Study on Electrodeposition of Aluminum and Aluminum-Manganese Alloys

A. Ispas,[a,*,z] E. Wolff,[b] and A. Bund[b,*]

[a]*Technische Universität Ilmenau, Chemistry Group, 98693 Ilmenau, Germany*
[b]*Technische Universität Ilmenau, Electrochemistry and Electroplating Group, 98693 Ilmenau, Germany*

The electrodeposition process of aluminum and aluminum-manganese alloys was studied in situ, by using an electrochemical quartz crystal microbalance, EQCM, with damping monitoring, in $AlCl_3$ based ionic liquids. Cyclic voltammetry, potentiostatic and galvanostatic deposition were performed at different temperatures, from 25°C up to 100°C. The morphology of the deposits was investigated by SEM and AFM, and their composition by EDX. The stoichiometry of the alloys was calculated from the EQCM data, based on Sauerbrey's equation. We could show that for thin films electrodeposited on gold electrodes, one can tune their morphology, and in the case of the alloys, also their composition, by modifying the deposition current or potential, as well as by modifying the temperature of the electrolyte. The morphology of the deposits changed gradually with increasing the amount of Mn in the electrolyte from a polyhedral like structure for Al films to round granules for the AlMn alloys. The mechanism for electrodeposition and dissolution of Al and AlMn alloys were analyzed and discussed based on the EQCM data.

Manuscript submitted March 30, 2017; revised manuscript received May 26, 2017. Published June 10, 2017. *This paper is part of the JES Focus Issue on Progress in Molten Salts and Ionic Liquids.*

Some of the chemicals used nowadays in industrial applications are toxic and/or environmentally benign. Alternatives are searched for those chemicals both by industry, as well as in academia. One of the metals of concern is Cd. Its corrosion and wear behavior are excellent. However, it is one of the metals of high concern for our health. According to some recent reports published by the Rowan Technology Group,[1] one promising alternative to replace Cd layers which could offer similar properties to these coatings are Al and Al alloys, in particular Al-Mn.[2] It was previously shown that alloying of Al with Mn produces layers that have better corrosion resistance[3,4] and improved mechanical properties[5] compared to pure Al films. This was the reason for choosing in this paper Al and AlMn alloys for a detailed study. The aim was to understand better the effect of the deposition parameters on the properties of the deposited films.

Electrodeposition of aluminum and its alloys has been intensively studied both in molten salts,[4,6] as well as in ionic liquid[7–12] electrolytes. Electroless deposition of Al films in room temperature ionic liquids has also been recently reported.[13] The reason for the interest in obtaining dense and uniform aluminum films is due to the special properties of this metal and its alloys, such as good corrosion resistance and wear resistance, light weight, and other more.[14] Thus, Al is well known to self-passivate in air, which means it forms an oxide layer that protects it from further corrosion. Aluminum and its alloys can be used in both decorative and functional coatings.

Different types of electrolytes were used for electrodeposition of Al and its alloys, such as organic electrolytes (toluene in the SIGAL process),[14] molten salts (such as $Li^+/K^+/AlCl_3$ eutectic system)[14] and ionic liquids (with ammonium, pyrrolidinium and imidazolium based cations).[14] The source for deposition of aluminum is triethyl aluminum in the SIGAL process, and mostly $AlCl_3$ in the others processes. Due to reactivity of the aluminum salts to even small amounts of moisture, the deposition process cannot be performed in ambient air without some special cell designs,[15] but it works straightforward in the inert atmosphere of a glove box.

Aluminum can be easily deposited from first generation ionic liquids (ILs), called chloroaluminate ionic liquids, obtained by mixing of $AlCl_3$ with 1-ethyl-3-methylimidazolium chloride, [EMIm]Cl. If the metal salt, $AlCl_3$, is present in molar excess, then the chloroaluminate is said to present Lewis acidity. If the organic salt is in molar excess, then it is said to be Lewis basic. Due to the simplicity of this process in chloroaluminate ionic liquids, these ILs were chosen also as electrolytes in this study.

Electrochemical Quartz Crystal Microbalance, EQCM, is a sensitive in situ technique, that gives the deposited mass on a metal electrode of an oscillating quartz crystal.

Sauerbrey described how the resonance frequency of a quartz crystal can change when a foreign mass is deposited on the top of the oscillator[16] (Eq. 1).

$$\Delta f = -\frac{2 f_0^2}{Z_q} \Delta m \qquad [1]$$

where Δf represents the shift in the resonance frequency of the quartz crystal when a rigid mass density, Δm, is deposited on one side of the resonator, Z_q is the mechanical impedance of quartz ($Z_q = (\mu_q \rho_q)^{1/2}$, with μ_q being the shear modulus and ρ_q being the density of the quartz crystal) and f_0 is the resonance frequency of the unloaded quartz. Thus, by measuring the shift of the resonance frequency of the quartz crystal, one can obtain in situ the mass that is deposited on it. In order to apply Eq. 1, some conditions should be fulfilled, such as the deposited film should be rigid and smooth. Moreover, it is well known that not only an additional mass will induce a frequency shift of a quartz resonator. Immersion of the quartz crystal in a very viscous liquid, like most ILs are, or changes in the viscoelastic properies of the liquids adjiacent to the quartz, will also induce changes of its resonant frequency, that can be mistaken as a mass change. It is very important thus to be able to separate the effects due to mass increase from the viscoelastic or roughnening of the surface effects. Our EQCM system is able to get both the shift of the resonance frequency as well as the disipated energy in terms of full witdh at half maximum, FWHM, of the resonance spectrum, which is proportional to the damping of the quartz. As a rule of thumb, if the shift in the resonance frequency is much bigger than the shift in damping, Eq. 1 can be applied. Otherwise, some corrections terms should be taken into account.[9,17,18]

The frequency of the quartz crystal depends also on temperature due to the change of its density and elastic modulus with temperature.[19,20] For some resonator types the change in frequency with temperature is rather large, so these quartzes cannot reach the

*Electrochemical Society Member.
[z]E-mail: adriana.ispas@tu-ilmenau.de

required frequency stability that is needed in some applications. In the case of AT-cut quartz crystals, one has a temperature coefficient close to zero around room temperature, but this can become more significant when the quartz crystals are used at higher temperatures. AT- and BT-cut quartz crystals belong to a class of so called X-cut quartzes, which means that they are obtained by cutting them from blocks in a direction perpendicular to the X-axis of the crystal. Cady reported a temperature coefficient of ca. $-20 \times 10^{-6}/^{\circ}C$ for the quartzes that are cut perpendicular to their X-axis, but around $90 \times 10^{-6}/^{\circ}C$ for the quartzes cut perpendicular to the Y-axis (such as CT- and DT-cut quartzes).[21] There are two possibilities to determine the temperature coefficient of the quartz crystals, namely, by modeling/simulations or by using in parallel two identical quartzes, from which one will be the reference, and the second one will be used in electrochemical measurements.[22] Often it is impossible to obtain two exactly identical quartzes. Therefore, in Ref. 22 the authors choose the modeling method with a cubic function for obtaining the compensation of temperature effects in the QCM measurements with AT-cut quartzes at high temperatures. The calculated frequencies as function of temperature were then compared to the measured values. Generally one is interested in the shift of the resonance frequency rather than in the absolute value of frequency. The shift of the resonance frequency due to the increase in temperature for an AT-cut quartz in air was approximately 800 Hz for the temperature range from 25 to 140°C[22] and around 200 Hz in a commercial grade pentaerythriol tetrapelargonate based lubricant.[22] Thus, it was proved that the QCM technique can be applied in viscous liquids at elevated temperatures such as up to 220°C. The sensitivity factor for the quartz crystal used (which is the coefficient between the deposited mass and the shift of resonance frequency in the Sauerbrey equation) changes with temperature. It was shown that it decreases linearly from 22.7 parts per million per degree at 65°C to 1.6 parts per million per degree at −189°C for the X-cut quartzes.[23] Threlfall reported for quartz crystals a temperature coefficient of stiffness of 0.000133 between 22 and 98°C, and an approximate coefficient of linear expansion of the quartz of 0.0000017 between 80°C and 36°C.[24] The adiabatic piezoelectric constants d_{11} and d_{14} were measured in Ref. 25 for α and β quartz at temperatures up to 626°C, and also in this case, one could notice that d_{11} and d_{14} do not change significantly from room temperature to 100°C. For the 10 MHz AT-cut quartz crystals that were used in this study, the sensitivity factor at room temperature is approximately 226 Hz μg^{-1} cm^2, and it decreases by 0.4% at 550°C. The value for density and shear modulus of the quartz at 550°C used in the above calculation were taken from Ref. 26. The temperature dependence of the density and shear modulus of the quartz crystal is thus relatively small in the range from 25°C to 100°C, so that the standard Sauerbrey equation (Eq. 1) can be applied in this temperature range without introducing significant systematic errors.

EQCM has been already applied for studying the electrodeposition of Al and its alloys in ionic liquids.[9,27–29] If imidazolium and pyrrolidinium based ILs were investigated in,[9] chloroaluminate ILs were studied in.[27–29]

When dissolving $AlCl_3$ in either 1-butyl-1-methyl-pyrrolidinium-bis(trifluoromethylsulfonyl)amide, [BMP][TFSA] or in 1-ethyl-3-methyl-imidazolium-bis(trifluoromethylsulfonyl)amide, [EMIm][TFSA] in a molar ratio of 1.6–2.5 or 2.5–5.0, respectively, a bi-phase separation was observed.[9] Interestingly, one could then obtain Al reduction only from the upper formed phase. Moreover, the nature of the cation influenced the crystal size of the deposits: microcrystalline films were obtained in the [EMIm] based IL, but nanocrystalline layers were obtained in the [BMP] based IL. EQCM measurements showed that the deposition/stripping of Al is reversible in [EMIm][TFSA], but irreversible in [BMP][TFSA]. In the viscous [BMP][TFSA] one could not apply Sauerbrey's equations for the measuremets performed at room temperature, but for those performed at 100°C one could get in situ the deposited mass. EQCM showed also the UPD (under potential deposition) of Al in [EMIm][TFSA] in the potential range from (+20 to −90 mV vs Al reference electrode) and OPD (over potential deposition) at more cathodic potentials.

Electrodeposition of Al,[27] Al-Cr,[27] Al-Co,[28] and Al-Mg[29] alloys were studied with EQCM in chloroaluminates ionic liquids at room temperaure. One could observe also in this case the UPD deposition of Al,[27] and interestingly, the deposition of Al-Cr[27] alloys set in at a potential more cathodic than that for deposition of Al, when the experiments were performed at room temperature. In the case of Al-Co electrodeposition,[28] EQCM indicated that the preferential composition of deposits is $CoAl_1$ and $CoAl_2$, depending on the deposition potential chosen, and that Al dissolves separetly during the anodic stripping from the Co from these alloys, a process that is also known as dealloying. The morphology of Al-Mg alloys electrodeposited at room temperature changed drastically with the current density.[29] The Mg content in the alloys was influenced by the current density chosen and by its initial concentration in the electrolyte.

Nucleation and growth of Al-Mn alloys on Pt electrodes was discussed in Ref. 30. The authors could show that the nucleation is in this case instantaneous. The growth of Al-Mn alloy is kinetically controlled at lower overpotentials, but it became diffusion controlled at higher overpotentials in a Lewis acidic $AlCl_3$: [EMIm]Cl ILs (1.2:1.0 and 2.0:1.0), with two $MnCl_2$ concentrations, namely, 25 mM and ca 200 mM, at room temperature.

In our previous paper[3] we discussed the deposition of Al and Al-Mn alloys on low carbon steel substrates, at room temperature, and we give some insights on the corrosion behavior of these deposits.

This paper will present the in situ EQCM results at room temperature as well as at higher temperature on electrodeposition of Al and AlMn alloys from Lewis acidic chloroaluminate ILs. A short discussion on the Lewis basic ILs will also be given.

Experimental

Anhydrous $AlCl_3$ (as ultra-dry powder, 99.99% or as granules, 99%) and $MnCl_2$ (99.99%) were purchased from Alfa Aesar and used as received, without further purification. [EMIm]Cl (>98%) was bought from Iolitec and dried at 70°C under vacuum for ca 16 h prior to utilization. Gold electrodes of ca 100 nm thickness evaporated on polished AT-cut quartz crystals with a resonance frequency of 10 MHz from KVG (Germany) were used as working electrodes. The electrochemically active area was 22.13 mm^2, and the active EQCM area was 19.63 mm^2. Aluminum wires (99+%) were used as counter and reference electrodes, respectively. A cell special designed for EQCM measurements at high temperatures was used. The temperature was applied on a resistive element and controlled by a thermocouple.

The frequency of the quartz crystal and its dissipated energy was measured with a network analyzer (Agilent E5100A).

A potentiostat model 263A from EG&G was used for electrochemical measurements. All experiments were performed inside an Omnilab glove box from Vacuum Atmosphere (USA), filled with Ar, with oxygen levels below 0.2 ppm and moisture below 0.5 ppm.

A Hitachi S-4800 scanning electron microscopy (SEM) equipped with an EDX detector (energy dispersive X-Ray analysis) was used for studying the morphology and the composition of the deposited layers. In some specific cases, the morphology and the roughness of the very smooth and shiny samples was characterized by Atomic Force Microscopy (AFM), with a Dimension Icon device from Bruker, in Scan Asyst measuring mode. The cantilevers used for these measurements had tips made out of silicon and fixed on nitride lever, with a resonance frequency of ca. 70 kHz and an elasticity constant of 0.4 N/m.

Results and Discussion

Cyclic voltammetry.—Cyclic voltammetry (CV) experiments were performed at 20 mV/s with the first sweep toward the cathodic direction (Fig. 1). Measurements were conducted at room temperature (ca 25°C), 50°C, 80°C and 100°C in the 2:1 $AlCl_3$: [EMIm]Cl electrolyte, and when 33 mM $MnCl_2$ or 0.2 M $MnCl_2$ were added to this electrolyte. In the following only the results obtained at RT and 100°C will be shown, in the 2:1 $AlCl_3$: [EMIm]Cl with and without 0.2 M $MnCl_2$.

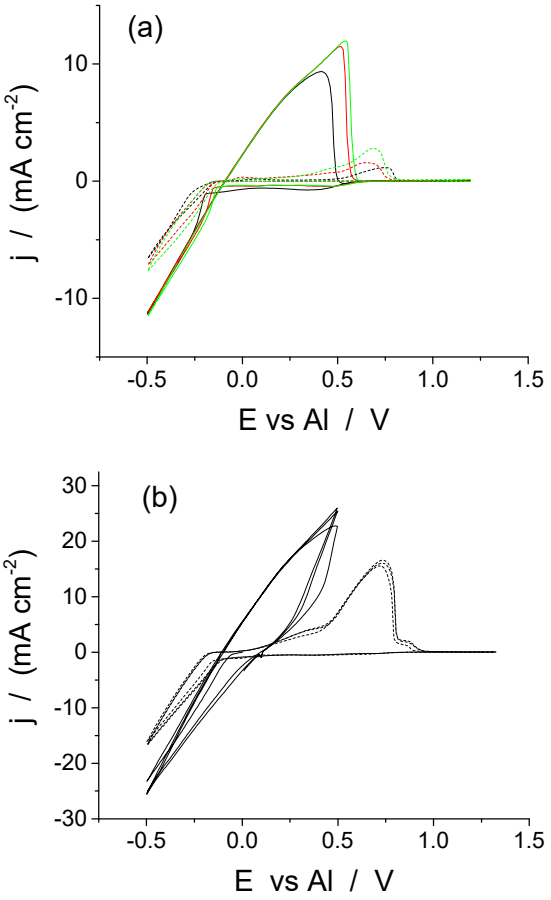

Figure 1. Cyclic voltammetry experiments at 20 mV/s in 2:1 $AlCl_3$: [EMIm]Cl (continuous line) and in 2:1 $AlCl_3$: [EMIm]Cl + 0.2 M $MnCl_2$ (dotted line) at room temperature (25°C ± 1°C) (a) and 100°C (b). The first cycle is depicted as a black line, the second one as red line and the third one as green line in Fig (a).

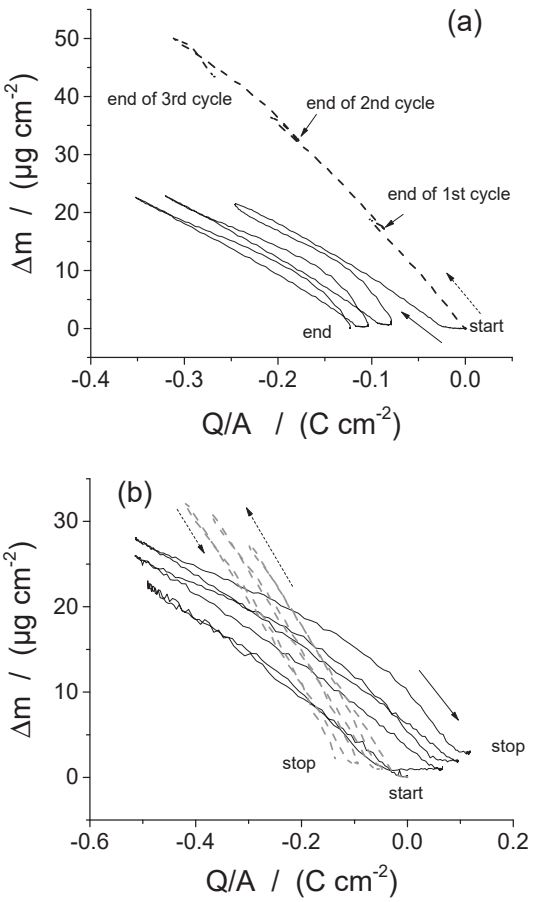

Figure 2. Mass-charge diagrams corresponding to the CV data presented in Fig. 1. Graph (a) corresponds to the measurements at RT, and graph (b) is for the measurements obtained at 100°C. Continuous line is for the pure Al deposition in 2:1 $AlCl_3$: [EMIm]Cl, and the dotted line is for 0.2M $MnCl_2$ in 2:1 $AlCl_3$: [EMIm]Cl.

One can notice in Fig. 1 that higher current densities were reached in the case of Al deposition/dissolution, as in the case of the Al-Mn alloy. Another interesting observation is that the deposition of Al seems to be chemically reversible: EQCM indicated that almost all the deposited mass in the cathodic sweep was removed during the anodic sweep (Fig. 2). However, the CVs performed in the presence of $MnCl_2$ showed that not all the deposited mass could be stripped away in the anodic sweep, even at elevated temperatures. This last fact can be due to irreversibility of the alloy deposition, which is often observed when depositing metals and alloys in ILs.[14] As one can notice in Fig. 1, the anodic stripping of Al occurs at more cathodic potentials than that of AlMn alloys. Thus, if an anodic potential limit of +0.5 V is enough to strip away most of the Al film deposited, one needs much higher anodic limit of potential for dissolution of the alloys. The anodic potential limits were chosen to +1.2 V in most of the cases, but they were only +0.5 V at higher temperatures for the electrolyte without $MnCl_2$. Even if more charge flows when depositing pure Al than for the AlMn alloys, due to the fact that AlMn does not completely dissolve when stripping it anodically, more charge and respectively, deposited mass, remains at the end of an experiment performed in similar conditions on the Au electrode for AlMn films. This fact is more obvious at RT (Fig. 2a) than at 100°C (Fig. 2b).

In both cases, Al and AlMn alloys, respectively, one can notice in the CVs that the current density increases with consecutive cycles. This fact is better visible in the anodic peak, and can be due to the increase of the active area of the electrode. Rests of deposited Al and AlMn that will remain on the Au electrode after the anodic stripping will make the surface of this Au electrode rougher and bigger than the initial surface of the Au electrode. With increasing the temperature of the electrolyte, the density of the electrolyte and its viscosity decrease, and the deposition process is facilitated. At the same time, the dissolution of the AlMn alloys seems to be easier at higher temperatures when compared to room temperature. This can be clearly seen both in Figs. 1 and 2, where the values of the current densities as well as the value of the final deposited mass increase with increasing the temperature. One can clearly see in Fig. 2 that the mass deposited and stripped after each cycle in the CV experiments for AlMn alloys is higher for each cycle at higher temperatures compared to RT. Of course, as at RT very few of the deposited alloy is stripped during the anodic sweep, the final mass of the deposit is higher in this case compared to that obtained at 100°C.

As previously shown in Refs. 28,29,31 one can estimate from the EQCM data the composition of the alloy deposited, or the stoichiometry of the deposited film. The slope of a mass-charge diagram, like those presented in Fig. 2, multiplied by the Faraday constant, F (96485 C mol^{-1}), will give a so called apparent molar mass, M_{app}. This M_{app} is in fact the ratio of a molar mass (with units of gram/mol) divided by the number of electrons transferred, z. The relative atomic mass of Al is 26.98, and that of Mn is 54.94. This means that if one considers that the deposition occurs at 100% current efficiency, one should get from the EQCM data an apparent molar mass of 8.99 g/mol if a pure Al layer ($z_{Al} = 3$) is deposited at a current efficiency of 100%, and 27.47 g/mol for a pure Mn layer ($z_{Mn} = 2$). In case of alloy formation, the following equations (Eq. 2) should indicate the stoichiometry of the Al, x_{Al} in the AlMn alloys, as calculated from the EQCM data, or

Table I. Apparent molar masses calculated from the CV experiments depicted in Fig. 1.

	1st cycle-deposition	1st cycle-dissolution before j_{anodic} = max	1st cycle-dissolution after j_{anodic} = max	2nd cycle-deposition	2nd cycle-dissolution before j_{anodic} = max	2nd cycle-dissolution after j_{anodic} = max	3rd cycle-deposition	3rd cycle-dissolution before j_{anodic} = max	3rd cycle-dissolution after j_{anodic} = max
Al; RT									
M_{app} (g/mol)	10.7	8.9	20.4	10.3	7.2	20.4	9.8	7.4	16.8
Al, 100°C									
M_{app} (g/mol)	5.0	4.0	6.0	14.3	20.9	27.0	14.5	20.2	32.0
AlMn; RT									
M_{app} (g/mol)	18.8	6.4	11.5	16.0	8.4	15.9	12.0	6.5	21.1
AlMn, 100°C									
M_{app} (g/mol)	9.6	11.6	-	9.3	10.6	12.2	9.6	8.7	12.0

more precisely, from the deposited mass, Δm:

$$M_{app}\,(alloy) = \frac{\Delta m}{Q_{total}} * F = x_{Al} * M_{app}\,(Al) + (1 - x_{Al}) * M_{app}\,(Mn) \quad [2]$$

The shift in resonance frequency, Δf, of the quartz crystal was generally much larger than the shift in FWHM for all the experiments performed. For example, in the CV experiments at RT for Al deposition, Δf was ca. 5 kHz, while the FWHM was ca. 150 Hz. This is a typical case when Eq. 1 can be applied without further corrections. The influence of the temperature on the resonance frequency of the quartz crystal was neglected in this work, as in Ref. 22 it was proved that for AT-cut quartzes and temperatures up to 140°C the shift in the resonance frequency induced by temperature (and measured both in air and in viscous media) is much smaller than the shift in the resonance frequency that we obtained in the electrochemical tests in this work (see detailed discussion above). The apparent molar mass calculated from the CV experiments at RT and 100°C for pure Al films and AlMn alloys are presented in Table I.

M_{app} is generally slightly higher than the theoretical value for the cathodic part in pure Al experiments (Table I), which indicates that Al might be deposited together with some other elements from the ionic liquid (see also discussion in the EDX section). At the same time, as presented in our previous paper,[3] at RT one often obtains quite rough Al films, where the layer grows as big plates. This is often observed for low current densities, below 6 mA/cm^2. One can have IL trapped between these big plates, and this extra-mass of IL trapped will be felt by the EQCM sensor. As a final effect, the M_{app} will deviate from the theoretical value that one should obtain for Al deposition at 100% efficiency. M_{app} obtained for Al deposition at 100°C is lower than the theoretical one in the first cycle, and it is higher in the consecutive cycles. We assume that this is due to the formation of some isolated Al grains on the Au electrode in the first cycle, surrounded by the IL that has a lower viscosity and density, due to the high temperature. Starting from the second cycle, one obtains a uniform film, that covers the entire surface of the electrode, and thus the M_{app} reaches values closed to that of theoretical Al films also in this case. The M_{app} was calculated also during dissolution experiments (Table I). The slope of the mass vs. charge diagram changes after the current density reaches its maximum in the anodic direction. Therefore, two values are reported in Table I for the anodic branch. As a general observation, one seems to dissolve pure Al till the current density reaches its maximum in its anodic sweep, and afterwards, a higher M_{app} is generally obtained. This last fact could be due to partial dissolution of the Au substrate, too, in this Cl^- containing IL, and at anodic potentials.

Equation 2 was applied in the case of AlMn alloys, for calculating the amount of Al in the alloys, x_{Al}. The obtained results for AlMn alloys are presented in Tables I and II. One can see that one can tune the Mn content in the AlMn alloys by modifying the electrochemical potential chosen for deposition. It seems that the electrodeposition of Al is favored when the temperature increases and at more cathodic potentials. Thus, in this case, the M_{app} is closer to the theoretical value for Al. It also seems that Al is dissolving preferentially firstly during the anodic sweep from the alloy, similarly as it was reported in Ref. 28 for Al-Co alloys. Before the maximum in the current density is reached in the anodic sweep, the value of M_{app} is closer to the theoretical value for Al, and it increases afterwards, showing that dissolution of Mn from the Al-Mn alloy, and finally, maybe some of the Au substrate dissolves, too.

Potentiostatic and galvanostatic deposition.—The EQCM measurements indicated that a mass increase can be detected starting from ca −0.1 V vs Al reference electrode. Therefore, potentiostatic depositions at −0.1 V (for 2 h), −0.2 V (for 1 h), −0.3 V (2400 s) and −0.5 V (for 1440 s) were performed at temperatures between RT and 100°C. The M_{app} was calculated also in this case from the EQCM data.

Galvanostatic depositions were performed for current densities between −0.1 and −10 mA cm^{-2}.

Aluminum films electrodeposited at −0.1 mA cm^{-2}, −1 mA cm^{-2} and −0.1 V showed a poor adherence on the Au electrode of the quartz crystal. The deposit for the conditions mentioned above was often in

Table II. Values for x_{Al} (Eq. 2) calculated in a series of CV experiments for AlMn deposition at room temperature. Here only the values from the cathodic scan are reported.

	1st cycle	1st cycle	1 st cycle	2nd cycle	2nd cycle	2nd cycle	3rd cycle	3rd cycle	3rd cycle
M_{app} (g/mol)	17.7	12.5	10.5	22.0	15.4	9.7	25.9	18.4	10.6
Potential region (V)	−0.18..−0.28	−0.32..−0.37	−0.38..−0.48	−0.15..−0.25	−0.28..−0.35	−0.38..−0.48	−0.13..−0.22	−0.25..−0.36	−0.4..−0.5
x_{Al}	0.5	0.8	0.9	0.3	0.6	0.9	0.1	0.5	0.9
Measurement 2									
M_{app} (g/mol)	16.4	11.3	-	22.4	16.5	10.4	28.9	16.5	10.1
Potential region (V)	−0.2..−0.25	−0.33..−0.5	-	−0.15..−0.25	−0.25..−0.35	−0.4..−0.5	−0.1..−0.17	−0.2..−0.3	−0.38..−0.5
x_{Al}	0.6	0.9		0.3	0.6	0.9	0	0.6	0.9
Measurement 3									
M_{app} (g/mol)	28.4	12.2	9.3	21.1	13.5	9.3	18.7	12.5	8.9
Potential region (V)	−0.02..−0.15	−0.28..−0.35	−0.4..−0.48	−0.1..−0.2	−0.25..−0.35	−0.45..−0.5	−0.1..−0.2	−0.3..−0.35	−0.4..−0.5
x_{Al}	0	0.8	1	0.3	0.7	1	0.5	0.8	1

form of powder. For the other experimental conditions chosen, one could obtain apparent molar masses between 7 and 9.5 g/mol, in case of potentiostatic depositions and current densities below 5 mA cm^{-2}. For higher current densities, such as 8 and 10 mA cm^{-2}, the M_{app} was bigger than the theoretical value for Al (namely, 10 and 18 g/mol). This fact indicated that at higher current densities, other elements from the electrolyte are incorporated in deposit besides Al.

One could notice often a change of slopes in the case of AlMn deposition, for potentiostatic and galvanostatic depositions. Generally, higher M_{app} values were obtained in the beginning of the deposition, and lower values at the end of deposition. This can be due to the stronger depletion in Mn ions than in Al ions of the electrolyte as the deposition experiment runs. Generally, a pretty fair agreement was obtained between the stoichiometry of alloy calculated with the EQCM data and the EDX results. Thus, for example, an AlMn electrodeposited for 1 h at −0.2 V at RT had an M_{app} of ca. 11.8 g/mol, which indicated an Al content of ca 84 At%. Indeed, EDX showed that this layer contains between 82 and 88 At% Al, on different regions on the electrode.

Morphology and composition of the deposits.—The morphology of the deposited layer shows a strong correlation with its composition. Thus, if $MnCl_2$ is added to the 2:1 $AlCl_3$: [EMIm]Cl, it will induce changes in the morphology of the deposits (Fig. 3). While plate like or pyramidal type morphologies were obtained for pure Al films[3] (Fig. 3), the morphology of the AlMn alloys changes into a granular type with increasing the Mn content. This fact was observed before by other groups, too. In Ref. 32, the authors mentioned that for films electrodeposited on Cu electrodes at RT and 6 mA cm^{-2}, one can clearly see angular or polyhedral-like structures if the Mn content is below 7.5 at% and rounded nodules for AlMn alloys containing more than 8 at% Mn. The change in the deposit morphology with increasing Mn content of the alloy can be correlated with changes in the crystallographic structure. The faceted structures correspond typically to microcrystalline films, while the round nodule structures indicate a nano-crystalline electrodeposit. Thus, by increasing the Mn content in the alloys, one could notice a change of the structure from a crystalline (fcc Al) to a mixed one, that contains both crystalline and amorphous phases, until finally, an amorphous phase is reached when the content of Mn exceeds 8 at% in AlMn alloys.[3,32]

It was shown in our previous paper[3] that the current density had a strong effect on the morphology of the deposited Al layers when deposited on low carbon steel at RT. Also on Au electrodes, one could notice that increasing the current density or the absolute value of the deposition potential, will induce smoother layers, both for pure Al layers, as well as for AlMn layers (Fig. 4). Increasing the temperature had a similar effect, namely, of reducing the roughness of the deposits (Fig. 5). However, the current density cannot be increased above some limits, without losing the quality of the deposits: for very high current densities, one does not obtain a good adherent layer anymore. This fact can be seen in Fig. 4, where in the case of Al films, the layer deposited at −0.5 V had worst visual appearance and morphology compared to layers till −0.4 V.

EDX analyses were performed for all deposited layers (Table III). One could notice that besides the two elements deposited, namely Al and Mn, one obtains sometimes impurities in the films in form of Cl or O. The chlorine comes from the electrolyte or the precursors used for deposition, and oxygen can come from the oxidation of these layers when exposed to air, during the transport between the glove box and the SEM/EDX device. In the case of thin AlMn films, by making the deposition potential or the current density more cathodic, one obtains smoother layers, but, at the same time, the amount of Mn detected in the films also increases. With increasing the temperature, one could also find less or even no O and Cl in the deposits (Table III) and more Mn. This fact is in agreement with the smoother and more compact morphology of the deposits that is obtained at higher current densities (Fig. 5).

The layers obtained at higher temperatures were very smooth and shiny. Due to that, it was challenging sometimes to obtain good SEM

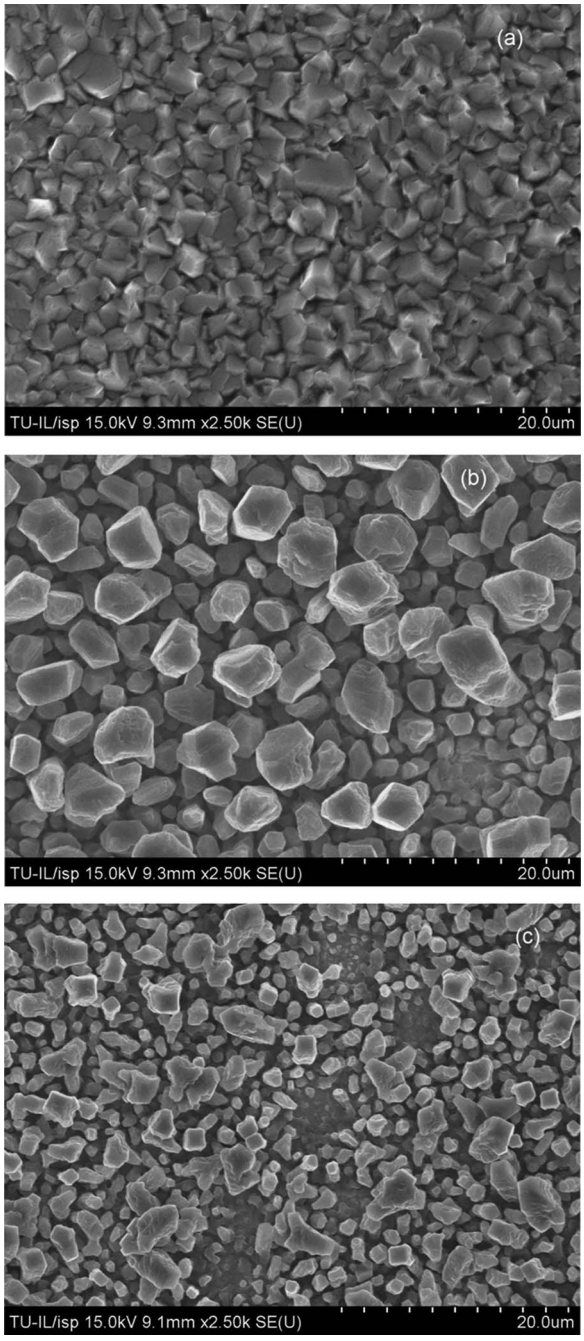

Figure 3. The effect of composition of electrolyte on morphology of the deposits. All experiments were performed at RT, 1 h at −0.2 V. Image (a) is a pure Al layer obtained from 2:1 $AlCl_3$: [EMIm]Cl, (b) is one AlMn layer obtained from 33 mM $MnCl_2$ in 2:1 $AlCl_3$: [EMIm]Cl and (c) is an AlMn layer obtained from 0.2M $MnCl_2$ in 2:1 $AlCl_3$: [EMIm]Cl.

images. For these samples, the morphology and the roughness of the deposited films was characterized also by AFM (Fig. 6). Five images were acquired in different regions of the deposited film. The roughness of the layer decreases by increasing the electrical potential used for deposition. The mean roughness, R_a for the layer depicted in Fig. 6a was between 3.7 and 4.1 nm, and between 2.1 and 3.5 nm for the layer shown in Fig. 6b. The mean roughness is the arithmetic average of the absolute values of the roughness profile ordinates. One can define another type of roughness, namely the root square mean roughness, R_q, which is in fact the root mean square average of the roughness profile ordinates. R_q was between 4.6 and 5.5 nm for the layer obtained

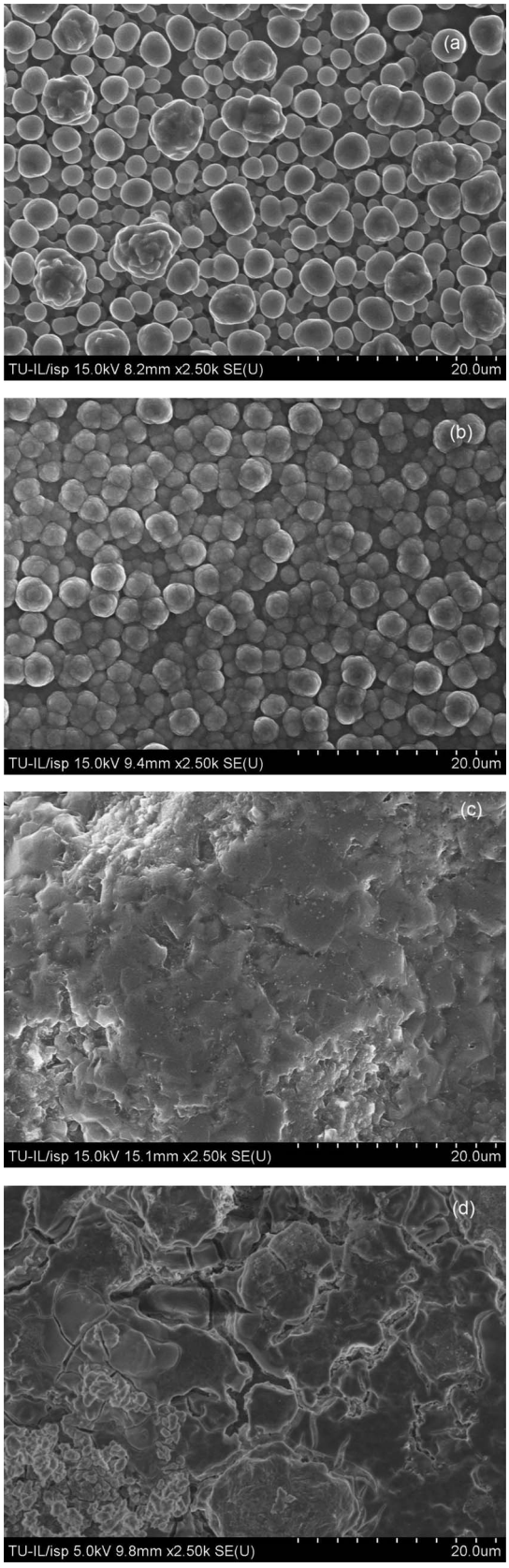

Figure 4. SEM images showing the effect of potential on AlMn and Al layers obtained at RT from 0.2 M $MnCl_2$ in 2:1 $AlCl_3$: [EMIm]Cl and in 2:1 $AlCl_3$: [EMIm]Cl, respectively. (a) AlMn, −0.3 V, (b) AlMn, −0.5 V, (c) Al, −0.3 V, (d) Al, −0.5 V.

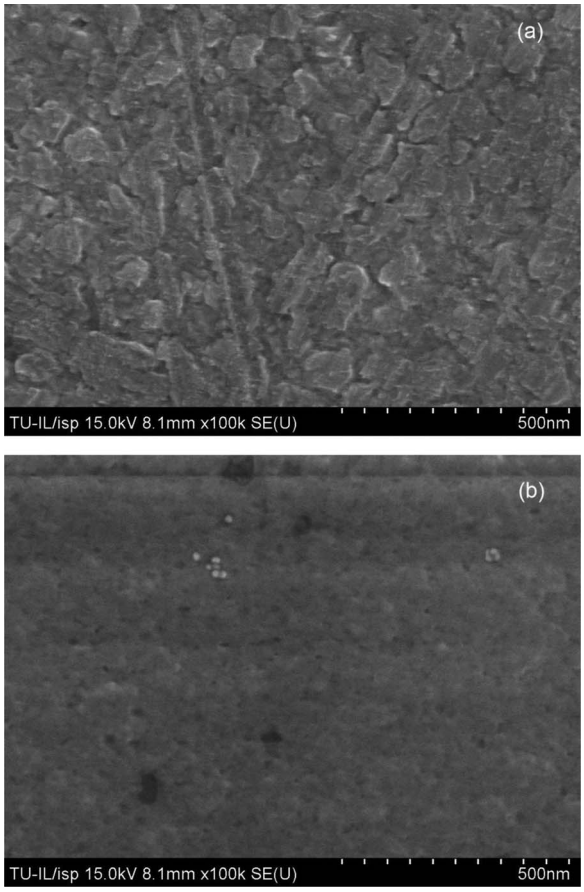

Figure 5. SEM image showing the effect of temperature on films deposited at 100°C and −0.2 V for 1 h. (a), Al layer, and (b) AlMn obtained from 0.2M $MnCl_2$ in 2:1 $AlCl_3$: [EMIm]Cl.

Table III. EDX results for some deposited layers.

Magnification	Al (at%)	Mn (at%)	O (at%)	Cl (At%)
AlMn from 0.2 M $MnCl_2$, RT, 1 h at −0.2 V				
1000x	84.9 ± 1.1	14.4 ± 1.7	0.3 ± 0.3	0.4 ± 0.3
2500x	82.8 ± 1.1	16.0 ± 1.7	1.0 ± 0.6	0.2 ± 0.2
AlMn from 0.2 M $MnCl_2$, RT, 2400 s at −0.3 V				
1000x	78.1 ± 1.3	21.5 ± 2.2	0.4 ± 0.4	0.0 ± 0.0
2500x	79.1 ± 1.4	19.9 ± 2.5	1.0 ± 0.8	0.0 ± 0.0
AlMn from 0.2 M $MnCl_2$, RT, 1440 s at −0.5 V				
1000x	74.5 ± 0.8	24.7 ± 2.5	0.0 ± 0.0	0.8 ± 0.2
2500x	77.3 ± 0.9	21.8 ± 2.6	0.0 ± 0.0	0.9 ± 0.2
AlMn from 0.2 M $MnCl_2$, 50°C, 1 h at −0.2 V				
1000x	77.6 ± 1.0	22.4 ± 2.5	0.0 ± 0.0	0.0 ± 0.0
2500x	78.7 ± 0.8	21.3 ± 2.5	0.0 ± 0.0	0.0 ± 0.0
AlMn from 0.2 M $MnCl_2$, 100°C, 1 h at −0.2 V				
1000x	73.3 ± 1.1	26.7 ± 2.7	0.0 ± 0.0	0.0 ± 0.0
2500x	75.5 ± 1.0	24.5 ± 3.3	0.0 ± 0.0	0.0 ± 0.0
Al, RT, 1 h at −0.2 V				
1000x	98.9 ± 1.3	-	1.1 ± 0.6	0.0 ± 0.0
2500x	97.8 ± 1.1	-	1.6 ± 0.6	0.6 ± 0.3
Al, RT, 1440 s at −0.5 V				
1000x	94.8 ± 1.0	-	5.2 ± 1.0	0.0 ± 0.0
2500x	94.5 ± 1.1	-	5.5 ± 1.0	0.0 ± 0.0
Al, 100°C, 1 h at −0.2 V				
1000x	100.0 ± 3.0	-	0.0 ± 0.0	0.0 ± 0.0
2500x	100.0 ± 1.5	-	0.0 ± 0.0	0.0 ± 0.0

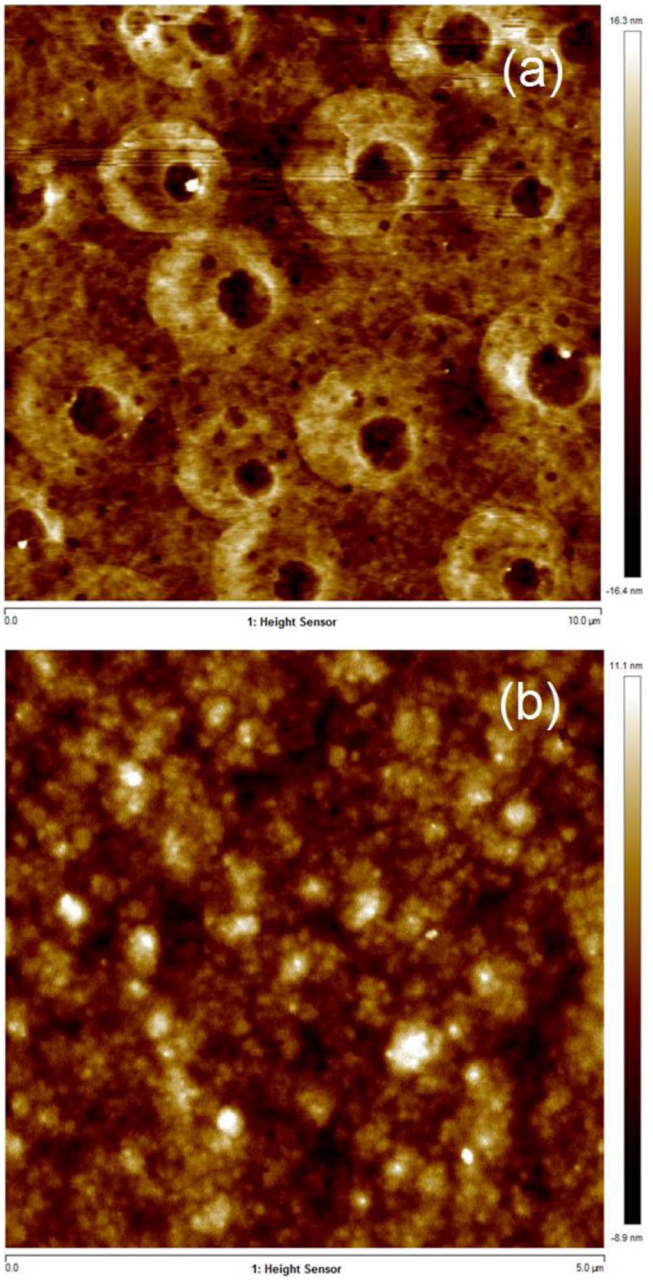

Figure 6. AlMn layers electrodeposited at 50°C from 0.2M $MnCl_2$ in 2:1 $AlCl_3$: [EMIm]Cl. Image (a) is for an electric potential of −0.2 V and image (b) is for −0.5 V.

at −0.2 V and 50°C and between 2.7 and 4.8 nm for the layer obtained at −0.5 V and 50°C.

EQCM investigations in Lewis basic ILs.—Some tests were performed in 1:1 $AlCl_3$: [EMIm]Cl and 1:2 $AlCl_3$: [EMIm]Cl ILs. These electrolytes are liquid at room temperature. We could dissolve 0.2 M $MnCl_2$ in both of them and we checked if in these electrolytes one could electrodeposit Mn films. The obtained results are presented in Fig. 7.

In the case of 1:1 electrolyte, two separated phase were formed. We checked therefore the electrochemical behavior of both the upper and the lower phase of the electrolyte and we compared the results obtained with the 1:2 electrolyte. One can see in Fig. 7, that in all three cases the shift in the resonance frequency of the quartz crystal, Δf, is much smaller than the shift of the FWHM, Δw. This is a typical case

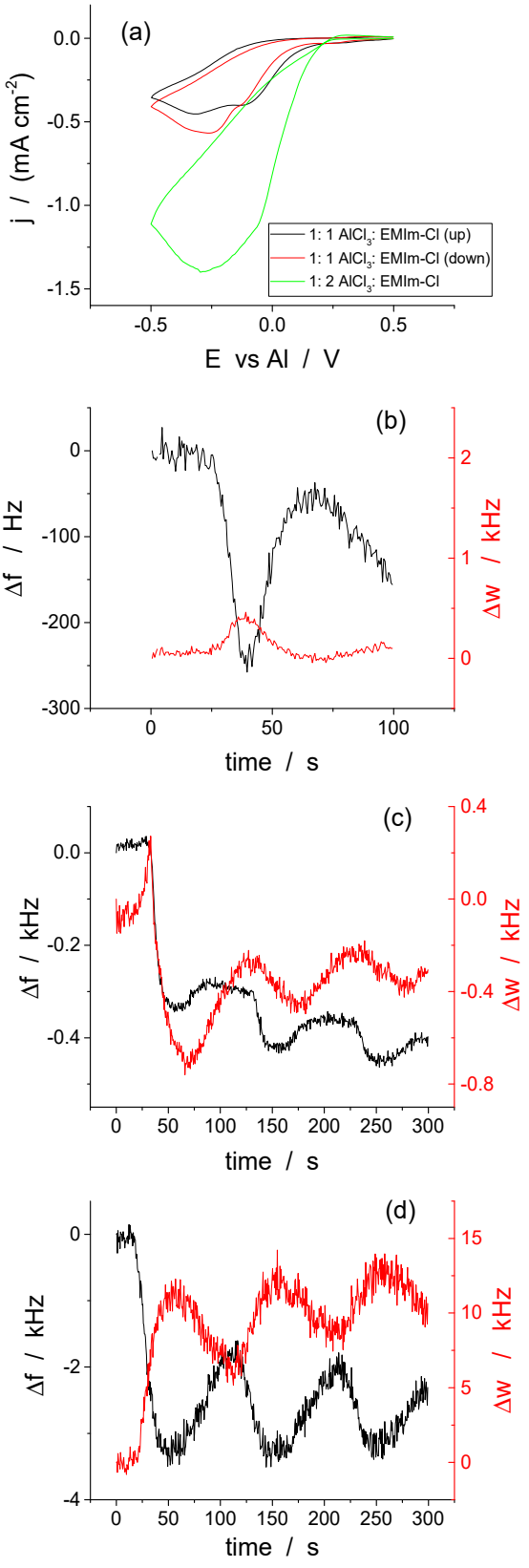

Figure 7. Cyclic voltammogram (a) experiments performed at RT and 20 mV s^{-1} in the upper phase of the 1:1 $AlCl_3$: [EMIm]Cl (black line), in the lower phase of the 1:1 $AlCl_3$: [EMIm]Cl (red line) and in 1:2 $AlCl_3$: [EMIm]Cl (green line). Graphs (b)–(d) present the shift in resonance frequency (black line) and the shift in FWHM (red line), here noted with Δw, for the upper phase of the 1:1 $AlCl_3$: [EMIm]Cl (b), in the lower phase of the 1:1 $AlCl_3$: [EMIm]Cl (c) and in 1:2 $AlCl_3$: [EMIm]Cl (d).

when the Eq. 1 cannot be applied directly to transform the shift of resonance frequency into deposited mass. Usually, the changes in Δf and Δw that one can see in Fig. 7 come from changes in viscoelastic properties of the electrolyte. Thus, the CVs experiments indicated that no deposited mass can be detected by EQCM in these two solutions. The same result was obtained if one keeps the potential of the working electrode at a cathodic limit for some time, such as −0.2 V or −0.5 V. Also in this case no deposit could be observed on the Au electrode.

Conclusions

Thin Al and AlMn films were electrodeposited on Au electrodes of quartz crystals from 2:1 $AlCl_3$: [EMIm]Cl ILs, with 33 mM $MnCl_2$ and 0.2 M $MnCl_2$.

One can tune the composition and the morphology of the thin AlMn deposits by modifying the current density and the temperature. Smooth and shiny surfaces could be thus obtained, without adding any extra additive to the bath.

EDX analyses showed that the deposited layers can contain sometimes impurities in the form of chlorine and oxygen. Increasing the temperature of the electrolyte increased the quality of the deposits. Their topography became smoother, and the amount of Cl and O impurities decreased, until it even vanished.

EQCM gave more insight in the deposition and dissolution mechanism of the Al and AlMn alloys. One could see that Mn rich film is firstly deposited in cyclic voltammogram measurements, and that during the anodic sweep the Al is dissolved preferentially first from the alloys. The stoichiometry of the deposited films can be calculated from EQCM data. The composition of the deposited alloy obtained from the EQCM data was compared to the composition of the films given by the EDX analyses.

One can deposit both Al and AlMn alloys from a Lewis acidic IL, but no Mn deposition could be observed from a Lewis basic ILs.

Acknowledgment

We thank for the financial support to the Federal Ministry of Economics and Energy (Bundesministerium Wirtschaft und Energie, BMWi), within the NiCO project (ref. no. 20W1523H) and to AiF (Arbeitsgemeinschaft industrieller Forschungsvereinigungen “Otto von Guericke” e.V.) within Alti2De project. EFRE (European Regional Development Fund) and DFG (German Research Foundation) are kindly acknowledged for financial support provided for the purchase of the AFM device.

References

1. K. Legg, *Cadmium Replacement Alternatives for the Joint Strike Fighter*, Rowan Technology Group, Libertyville, IL, USA, Report No. 3105JSF3 (2000).
2. M. Bielewski, Chapter 23 -Replacing Cadmium and Chromium. Research report, Ottawa, Ontario: Institute for Aerospace Research, National Research Council Canada, in RTO-AG-ATV-140: Corrosion Fatigue and Environmentally Assisted Cracking in Aging Military Vehicles, (2011).
3. A. Ispas, C. A. Vlaic, M. Camargo, and A. Bund, Electrochemical deposition of aluminum and aluminum-manganese alloys in ionic liquids, *ECS Trans.*, **75**(15), 657 (2016).
4. T. Moffat, G. R. Stafford, and D. E. Hell, Pitting Corrosion of Electrodeposited Aluminum-Manganese Alloy, *J. Electrochem. Soc.*, **140**(10), 2779 (1993).
5. S. Ruan and C. A. Schuh, Towards electroformed nanostructured aluminum alloys with high strength and ductility, *J. Mater. Res.*, **27**, 1638 (2012).
6. M. Ueda, Overview over studies of electrodeposition of Al or Al alloys from low temperature chloroaluminate molten salts, *J. Solid State Electrochem.*, **21**(3), 641 (2017).
7. T. Tsuda, T. Nohira, and Y. Ito, Nucleation and surface morphology of aluminum-lanthanum alloy electrodeposited in a $LaCl_3$ saturated $AlCl_3$-EtMeImCl room temperature molten salt, *Electrochem. Acta*, **47**(17), 2817 (2002).
8. T. Tsuda, C. L. Hussey, G. R. Stafford, and J. E. Bonevich, Electrochemistry of titanium and the electrodeposition of Al-Ti alloys in the Lewis acidic aluminum chloride-1-ethyl3-methylimidazolium chloride melt, *J. Electrochem. Soc.*, **150**, C234 (2003).
9. E. M. Moustafa, S. Z. El Abedin, A. Shkurankov, E. Zschippang, A. Y. Saad, A. Bund, and F. Endres, Electrodeposition of Al 1-buthyl-1-methylpyrrolidinium bis(trifluoromethylsulfonyl)amide and 1-ethyl-3-methylimidazolium bis(trifluorosulfonyl)amide ionic liquids: In situ STM and EQCM studies, *J. Phys. Chem. B.*, **111**, 4693 (2007).
10. A. P. Abbott, F. Qiu, H. M. A. Abood, M. R. Ali, and K. S. Ryder, Double Layer, Diluent and Anode Effects upon the Electrodeposition of Aluminium from Chloroaluminate based Ionic Liquids, *Phys. Chem. Chem. Phys*, **12**, 1862 (2010).
11. Y. Fang, K. Yoshii, X. Jiang, X.-G. Sun, T. Tsuda, N. Mehio, and S. Dai, AnAlCl3 Based Ionic Liquid with Neutral Substituted Pyridine Ligand for Electrochemical Deposition of Aluminum, *Electrochim. Acta*, **160**, 82 (2015).
12. S. Schaltin, M. Ganapathi, K. Binnemans, and J. Fransaer, Modeling of Aluminuim Deposition from Chloroaluminate Ionic Liquids, *J. Electrochem Soc.*, **158**(10), D639 (2011).
13. N. Koura, H. Nagase, A. Sato, S. Kumakura, K. Takeuchi, K. Ui, T. Tsuda, and C. K. Loong, Electroless Plating of Aluminum from a Room-Temperature Ionic Liquid Electrolyte, *J. Electrochem. Soc.*, **155**(2), D155 (2008).
14. Electrodeposition from Ionic Liquids. Edited by F. Endres, D. MacFarlane, and A. Abbott, (2008) WILEY-VCH Verlag GmbH & Co. KGaA, Weinheim, Germany, pp. 88–90; 125–133; 353–362.
15. A. Bakkara and V. Neubert, A new method for practical electrodeposition of aluminum from ionic liquids, *Electrochem. Commun.*, **51**, 113 (2015).
16. D. Johannsmann, “*The Quartz Crystal Microbalance in Soft Matter Research. Fundamentals and Modeling*,” Springer Cham Heidelberg New York Dordrecht London (2015).
17. V.-T. Gruia, A. Ispas, M. Wilke, I. Efimov, and A. Bund, Application of acoustic impedance method to monitoring of sensors: Metal deposition on viscoelastic polymer substrate, *Electrochim. Acta*, **118**, 88 (2014).
18. S. Ivanov, C. Vlaic, A. Bund, and I. Efimov, In situ analysis of surface morphology and viscoelastic effects during deposition of thin silicon layers from 1-butlyl-1-methylpyrrolidinium bis(trifluoromethylsulfonyl)imide, *Electrochim. Acta*, **219**, 251 (2016).
19. W. L Bond, The Mathematics of the Physical Properties of Crystals in *The Bell System Technical Journal*, **XXII**(1), 1 (1943).
20. I. Efimov, A. Ispas, and A. Bund, Taking into account of surface roughness for the calculation of elastic moduli of polymer films from acoustic impedance data, *Electrochim. Acta*, **122**, 16 (2014).
21. W. G. Cady, *Piezoelectricity*: Vol. 1, McGraw-Hill Book Company, New York (1946) and Vol. 2, Dover Publications (1964).
22. D. Wang, P. Mousavi, P. J. Hauser, W. Oxenham, and C. S. Grant, Quartz crystal microbalance in elevated temperature viscous liquids: Temperature effect compensation and lubricant degradation monitoring, *Colloids Surf. A.: Physicochem. Eng. Aspects*, **268**, 30 (2005).
23. R. S. Strout, The Temperature Coefficient of Quartz Crystal Oscillators, *Phys. Rev.*, **22**, 829 (1928).
24. R. Threlfall, The Elastic Constants of Quartz Threads, *Phil. Mag.*, **30**, 99 (1890).
25. R. K. Cook and P. G. Weissler, Piezoelectric Constants of Alpha – and Beta-Quartz at Various Temperatures, *Phys. Rev.*, **80**(4), 712 (1950).
26. W. Pabst and E. Gregorová, Elastic Properties of Silica Polymorphs- A Review, *Ceramics – Silikáty*, **57**(3), 167 (2013).
27. H. C. De Long and P. C. Trulove, EQCM Studies of Aluminum and Aluminum Alloys in Room Temperature Molten Salts, *Electrochemical Society Proceedings*, **96–7**, 276 (1996).
28. H. C. De Long and R. T. Carlin, EQCM Measurements of Cobalt-Aluminum Alloys, *Electrochemical Society Proceedings*, **96–7**, 284 (1996).
29. M. R. Ali, A. P. Abbott, and K. S. Ryder, Electrodeposition of Al-Mg Alloys from Acidic $AlCl_3$-EMIC-$MgCl_2$ Room Temperature Ionic Liquids, *J. Electrochem.*, **21**(2), 172 (2015).
30. H. C. De Long, J. A. Mitchell, P. L. Hagans, R. T. Carlin, G. R. Stafford, and P. C. Trulove, Electrodeposition of Aluminum-Manganese Alloys from Room Temperature Chloroaluminate Molten Salts, *Electrochemical Society Proceedings*, **98–11**, 40 (1998).
31. A. Ispas, A. Bund, and F. Endres, Application of the Electrochemical Quartz Crystal Microbalance for the Investigation of Metal Depositions from Ionic Liquids, *ECS Trans*, **16**(49), 411 (2009).
32. S. Ruan and C. A. Schuh, Electrodeposition Al-Mn alloys with microcrystalline, nanocrystalline, amorphous and nano-quasicrystalline structures, *Acta Materialia*, **57**, 3810 (2009).